THE AMERICAN SOCIETY OF MECHANICAL ENGINEERS
345 E. 47th St., New York, N.Y. 10017

96-TA-7

HEAT TRANSFER PREDICTIONS FOR U-SHAPED COOLANT CHANNELS WITH SKEWED RIBS AND WITH SMOOTH WALLS

Bernhard Bonhoff
Uwe Tomm
Bruce V. Johnson
ABB Corporate Research
CH - 5405 Baden-Dättwil,
Switzerland

ABSTRACT

A computational study was performed for the flow and heat transfer in coolant passages with two legs connected with a U - bend and with dimensionless flow conditions typical of those in the internal cooling passages of turbine blades. The first model had smooth surfaces on all walls. The second model had opposing ribs staggered and angled at 45° to the main flow direction on two walls of the legs, corresponding to the coolant passage surfaces adjacent to the pressure and suction surfaces of a turbine airfoil. For the ribbed model, the ratio of rib height to duct hydraulic diameter equaled 0.1, and the ratio of rib spacing to rib height equaled 10. Comparisons of calculations with previous measurements are made for a Reynolds number of 25,000. With these conditions, the predicted heat transfer is known to be strongly influenced by the turbulence and wall models. The k-e model, the low Reynolds number RNG k-e and the differential Reynolds-stress model (RSM) were used for the smooth wall model calculation. Based on the results with the smooth walls, the calculations for the ribbed walls were performed using the RSM and k-e turbulence models. The high secondary flow induced by the ribs leads to an increased heat transfer in both legs. However, the heat transfer was nearly unchanged between the smooth wall model and the ribbed model within the bend region. The agreement between the predicted segment - averaged and previously - measured Nusselt numbers was good for both cases.

NOMENCLATURE

C_μ	turbulence modeling constant
d_H	hydraulic diameter
e	rib height
k	turbulence energy
m	coolant flow rate
Nu, Nu_∞	Nusselt number
p, Δp	pressure
P	rib spacing pitch
Q_{in}	dynamic head at the inlet
r_i	inner bend radius
Re	Reynolds number
T, T_b	temperature
v, v_b	velocity magnitude
y^+	dimensionless wall distance

Greek symbols

α, α_0	inverse Prandtl number
ε	dissipation rate
μ_t	turbulent dynamic viscosity
ν_{eff}	effective kinematic viscosity
ν_{mol}	kinematic viscosity
θ	blending parameter
ϕ	variable
ρ	density
σ_θ	Prandtl number
σ_k	Prandtl number for turbulent transport
τ_t	wall shear stress

Subscripts

b	bulk
0, ∞	reference condition

INTRODUCTION

The needs for cooling gas turbines have increased steadily as the differences between turbine inlet and allowable metal temperatures increase. The turbine inlet temperatures for industrial and aircraft gas turbines have increased approximately 25 to 30 C° per year for the past 20 years. The allowable metal temperatures have also increased but at a slower rate. In addition, the compressor pressure ratios have also increased with the result that coolant air available has higher temperatures than for previous

Presented at the 1996 ASME Turbo Asia Conference
November 5–7, 1996 — Jakarta, Indonesia

applications. Continued use of the same airfoil cooling technology as the compressor discharge air temperature increases results first in no increase in power plant efficiency with increasing burner temperature. In addition to the need for using the cooling air efficiently to avoid performance penalties, the gas turbine designer is also under pressure to develop cooling configurations with a minimal number of laboratory, cascade or "rainbow wheel" tests.

Numerical modeling of the flow and heat transfer in the blade coolant passages has been long sought as an accurate, rapid and, therefore, cost effective method of predicting local and averaged heat transfer distribution in rotating and stationary coolant passages. The current ideal procedure would have a designer make coolant passage geometric changes one day and have accurate numerical heat transfer results the next morning showing the net effect of that change on the airfoil temperature and life characteristics. Practical coolant passages include the use of heat transfer enhancing trips or ribbons at various angles to the mean flow direction in a multipass serpentine configuration in a rotating environment with rotating gravitational forces 10,000 to 40,000 times the earth's "g" force. The flow and heat transfer in these passages can be dominated by turbulent flow, the enhanced surface characteristics, the Coriolis effects or the buoyancy effects. Experimental results, showing dimensionless flow and thermal boundary conditions for all the aforementioned effects, were presented by Johnson et al (1994).

Thus far, most of the published numerical effort has been directed toward obtaining accurate heat transfer predictions in smooth stationary and rotating coolant channels, (e.g., UMIST , GE, U of Swansea, Texas A&M, Carnigie Mellon). Reviews of the efforts to predict heat transfer in these channels were presented by Iacovides and Launder (1995) and by Prakash and Zerkle (1994). The reader is referred to their reviews for a details of previous work and to Bo et al. (1995) for a general discussion of the code algorithms and turbulence models .

Few predictions have been presented for rotating coolant passages with enhanced heat transfer surfaces with ribbons or trips. Taylor et al. (1991) showed the effects of annular ribs in a rotating cylindrical tube. A finite element method code, developed at Swansea, was employed as well as "ad hoc" relationships for the turbulent Prandtl number at various values of y^+ less than 25. Calculations were performed for a flow with a Reynolds number of 15,000 and a rotation number of 0.04 with a constant density fluid. The calculated results were in good agreement with the experimental measurements. Abuaf and Kercher (1994) presented a numerical / experimental comparison of flow and heat transfer in a stationary large scale model of a gas turbine blade containing a three pass serpentine passage with ribs normal to the flow direction. The computations were performed at ADAPCO with the STAR-CD code using a k-ε turbulence and a standard wall shear model. Results from the calculations were scaled to experimental conditions for the comparison. The trends for the heat transfer and turbulence levels in the serpentine passage were well predicted although the absolute levels of the local heat transfer prediction varied with grid size. Predictions with a fine grid and scaled to the experimental conditions were in good agreement with the experimental results. Prakash and Zerkle (1993) have predicted flow and heat transfer in a ribbed rectangular duct with and without rotation, using a k-ε turbulence model and standard wall functions. For all these previous calculations, the ribs were normal to the flow and buoyancy effects were neglected. Selected comparisons with correlations from the literature for stationary passages and with results from proprietary rotating experiments for rotation numbers of 0.0, 0.06 and 0.12 were satisfactory. Prakash and Zerkel (1993) also reviewed results from earlier exploratory calculations with ribs.

Although many advanced gas turbine coolant passage designs employ ribs at angles of 45 to 70 degrees to the coolant flow direction, the previous calculations for flow in ribbed coolant passages cited has been for ribs normal to the flow direction and usually with buoyancy neglected. As shown by Johnson et al. (1993, 1994), ribs normal to the flow can be sensitive to buoyancy effects for high rotation numbers and especially for flow inward. As a result, the present effort was directed toward the evaluation of calculation procedures with skewed rib configurations and with the inclusion of both Coriolis and buoyancy effects. These evaluations have been conducted for the experimental conditions of coolant passages without rotation and with smooth walls or walls with skewed trips, presented by Wagner et al. (1991) and Johnson et al. (1994) and available as NASA reports, Hajek et al.(1991) and Johnson et al. (1993). The present calculations were obtained using the FLUENT commercial code. Calculations have been completed for the smooth wall conditions using several turbulence models and for the walls with skewed trips using the k-ε model and the Reynolds stress equations. This paper presents the flow characteristics and heat transfer results from the calculations and compares the heat transfer predictions with the experimental results cited for no rotation. The predicted flow characteristics show the magnitudes of the secondary flows in the coolant passages and the thermal mixing mechanisms.

ANALYTICAL MODEL

In this paragraph the solution process and the turbulence models that were used in this study are described very briefly. A detailed description of the theory can be found in the FLUENT manual.

Overview

The governing equations of continuity, momentum and energy were solved using the finite volume code FLUENT version 4.3.2. This is a pressure based procedure which solves the full Navier-Stokes equations in general, body-fitted coordinates. A non-staggered, control-volume storage scheme is employed and all variables are stored at the cell center. In this study, a blended upwind/central difference scheme is used to interpolate the values of the cell faces. This scheme provides accuracy for the spatial discretization up to third order, depending on the choice of the parameter θ in equation 1 which bounds the scheme in order to avoid numerical instabilities like oscillations or overshoots. The

bending parameter θ is computed depending on the relative maximum of the adjacent cell center values.

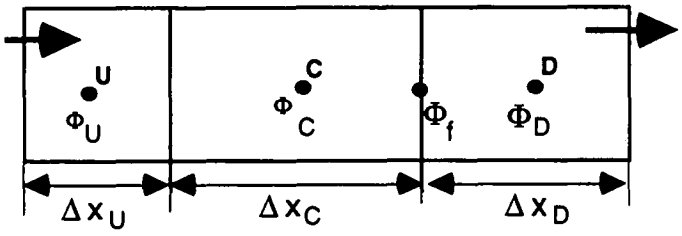

Fig 1: Higher order discretization

$$\phi_f = \theta \cdot \left[\frac{\Delta x_D}{\Delta x_C + \Delta x_D} \phi_C + \frac{\Delta x_C}{\Delta x_C + \Delta x_D} \phi_D \right] + (1-\theta) \cdot \left[\frac{\Delta x_U + 2\Delta x_C}{\Delta x_U + \Delta x_C} \phi_C + \frac{\Delta x_C}{\Delta x_U + \Delta x_C} \phi_U \right] \quad (1)$$

To solve the equations of continuity and momentum, the pressure-velocity coupling algorithm SIMPLE is employed. The iterative solution procedure is carried out by a Line Gauss-Seidel elimination technique. A multigrid technique is used to decrease calculation times.

Turbulence models.

To take turbulence effects into account, a turbulence model for the turbulent viscosity is needed. A number of turbulence models have been developed in the last few years. Some of them are only slightly different. The following turbulence models with fundamental differences are incorporated into the FLUENT Version 4.3.2 code:

- k-ε model (standard)
- ReNormalisation Group (RNG) k-ε model
- Reynolds Stress model (RSM)

The main aspects of these turbulent models, all used for comparison in the present study, are briefly described below. A more detail description of the models can be found in the FLUENT Manual, in Launder and Spalding (1972), Rodi (1984), Yakhot and Orszag (1986), Launder et al. (1975) and Launder (1989).

k-ε turbulence model. The equation for the turbulent transport k and its dissipation, ε ,are derived from the time-averaged momentum equations. The Boussinesq hypothesis is employed to express the Reynolds stresses. The turbulent viscosity μ_t is obtained by assuming that it is proportional to the product of a turbulent velocity scale and a length scale. The turbulence energy k and its dissipation, ε, are used to express this product in the k-ε turbulence model. In equation (2) the turbulent viscosity is given by:

$$\mu_t = \rho \cdot C_\mu \cdot \frac{k^2}{\varepsilon} \quad (2)$$

The non-equilibrium wall-function formulation is used with this k-ε turbulence model. In contrast to the standard wall-function the non equilibrium wall functions employs a two-layer concept in which wall neighboring cells are assumed to consist of a viscous sub layer and a fully turbulent layer. Depending on the thickness of the viscous sub layer the shear stress τ_τ, turbulence energy k and its dissipation ε are described using different profiles for the two layers. The heat transfer at walls is computed via a log-law formulation based on the analogy between heat and momentum transfer, Launder and Spalding (1973).

Re Normalization Group (RNG) k-ε turbulence model. The RNG k-ε model follows the two equation turbulence modeling framework and has derived from the original governing equations for fluid flow using mathematical techniques called Re normalization Group methods (Yakhot and Orszag (1986)). Through a scale elimination procedure that removes iteratively narrow bands of modes from the wide range of turbulent length scales and by expressing these modes in modes of inertial range eddies, an equation for the variation of effective viscosity with the Reynolds Number is developed. FLUENT's implementation of the RNG model includes a variation of the Prandtl number for turbulent transport σ_k, that allows the k and ε transport equation to be applied in low-Re number regions without involving wall functions or ad hoc damping functions:

$$\frac{\nu_{mol}}{\nu_{eff}} = \left| \frac{\alpha - 1.3929}{\alpha_0 - 1.3929} \right|^{0.6321} \left| \frac{\alpha + 2.3929}{\alpha_0 + 2.3929} \right|^{0.3679} \quad (3)$$

with α being the inverse Prandtl number for turbulent transport and α_0 set to $\alpha_0 = 1$. When this low-Re extension is used the turbulent viscosity and the Prandtl number vary smoothly with the effective Reynolds number from molecular to fully turbulent values. The RNG k and ε transport equations include a natural damping effect in the near wall region. The low-Re RNG model can be used with and without wall functions depending on whether the nearest wall node lies in the sub layer. When the low-Re extension is used, the heat fluxes are computed by means of the calculated node temperatures.

Reynolds Stress turbulence model. The RSM algorithm performs the calculation of the individual Reynolds stresses via differential transport equations. The transport equations are obtained from the momentum equations and contain triple order velocity correlations and pressure velocity correlations, that must be modeled to provide closure. FLUENT's implementation of the RSM contain assumptions of Launder et al. (1975) and Launder (1989). The turbulent viscosity is computed via equation (1) by determining k and ε in assistance with the calculated individual stresses. For the near wall treatment standard equilibrium wall functions are used to compute the shear stresses and to set the near wall boundary conditions for the individual stresses. The heat transfer at the wall is computed by means of the same wall function formulation, which is also used for the k-ε turbulence model. The calculations with k-ε model and RSM are performed using the standard turbulence modeling constants, except the turbulent Prandtl number is taken to $\sigma_\theta = 0.9$.

CONFIGURATION

In Fig. 2 the rectangular four pass, serpentine passage with three 180° turns, that was experimentally investigated by Wagner et al. (1991) and Johnson et al. (1994) is given.

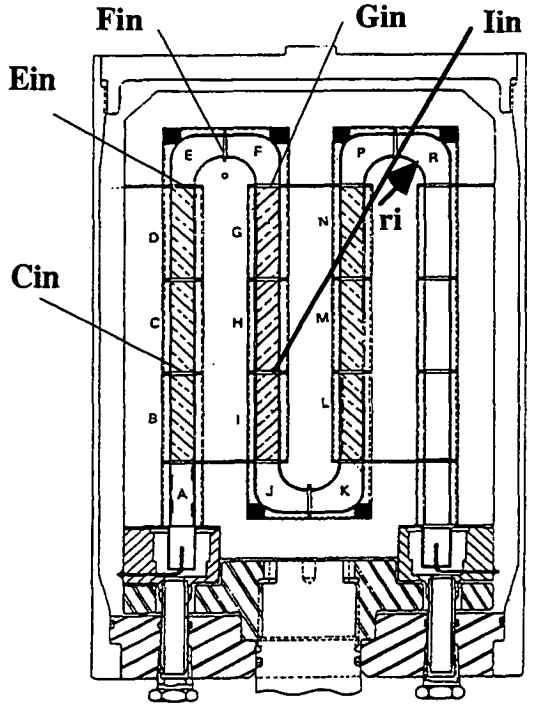

d_H = 12.7 mm, e / d_H = 0.1, P / e = 10, r_i / d_H = 1.25

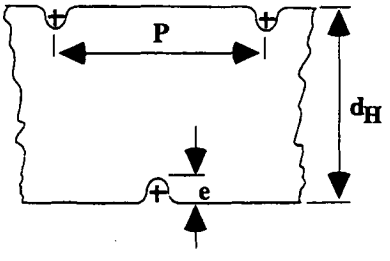

Fig. 2: Cross sectional view of coolant passage heat transfer model assembly with skewed ribs

This turbine blade passage geometry was chosen, because a comprehensive set of heat transfer measurements was provided. Measurements were made for the stationary and rotating duct with smooth walls and with walls having normal or skewed, staggered ribs. The duct has a rectangular cross section with d_h = 0.0127 m square. The other geometrical dimensions are listed Fig. 2. The first three straight legs of the serpentine and the turns are heated to a constant temperature, while the fourth leg and inner walls of the turns are covered with thermal isolation. For all sections, marked A to R in Fig. 2, constant temperature steady state heat balance measurements and wall static pressure measurements were made. In the present study the flow field and the transfer is simulated for the first two passages with the turn. For comparisons the measured side-averaged Nusselt numbers and the measured static pressure are used.

GRID GENERATION

Calculations were performed for the two passage cooling channel with:

- smooth walls
- 45° angled ribs, staggered on the upper and the lower sides of the straight sections.

Different grids are used in order to achieve the requirements for the different turbulence models concerning the y^+ values of the nearest wall nodes. For the k-ε model and the RSM, both with wall functions, a y^+ of about 30 and for the RNG model without wall functions, a y^+ of about 4 is recommended. Thus, a grid with 21x21 grid points in each cross section was set up for the k-ε turbulence model and the RSM and 27x27 grid points were used for the low- Re RNG turbulence model, respectively.

For the duct with smooth walls 220 grid lines are used in stream wise direction with 88 lines in the first leg, 52 lines in the bend and 80 lines in the second leg. 482 grid lines are employed in stream wise direction for the ribbed duct with 218 lines in the first leg, 44 lines in the bend and 220 lines in the second leg. Fig. 3 shows some details of the grid for the ribbed duct. To resolve the shape of the round ribs, at least 9 grid points are necessary for the approximation of each rib.

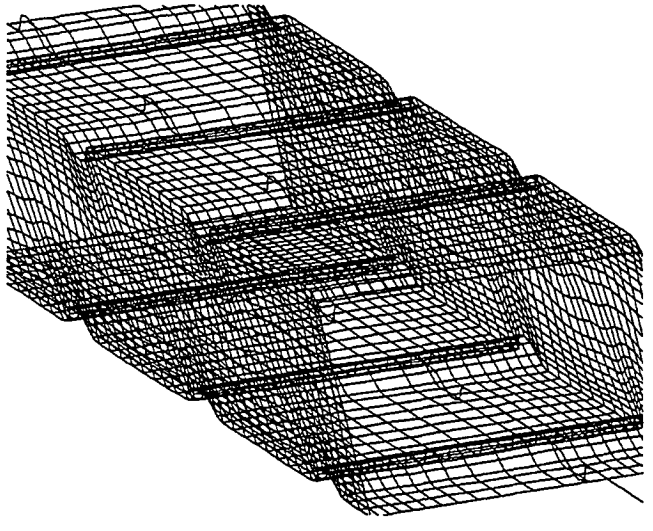

Fig. 3: View in a ribbed section

BOUNDARY CONDITIONS

From the various experiments, those with conditions, typical of modern industrial gas turbines, are chosen for the present numerical investigations.

Re = 25000, m = 0.0059 kg/s, p = 10.17 bar, T = 300.24 K.

Unlike the experiments, a uniform velocity profile is assumed at the inlet with a turbulence level of 3%. . A zero normal gradients

exit boundary condition is set. The density and the properties of the fluid are taken as a function of the temperature. A piece wise linear expression is used for their dependence on the temperature. At the wall, a uniform temperature is prescribed to be equal 344.64 K, i. e. $\Delta T = 44.4$ K. As mentioned before, the inner surface of the bend and the heat transfer section J is unheated.

RESULTS AND DISCUSSION

In the present study the flow and heat transfer in cooling channels is investigated by CFD. Table 1 gives an overview of the calculated cases and the turbulence models that were used.

configuration / turbulence model	smooth walls	ribbed walls
standard k-e	x	x
low-Re-RNG k-e	x	-
Re-Stress	x	x

Table 1: Configurations and turbulence models

The main objectives of this study are:

- to understand the physics of the flow in the straight sections with ribs and in the bend
- to test different turbulence models with regard to their heat transfer prediction capabilities
- to obtain a qualitative description of the local heat transfer

For the discussion of the flow structures and the local heat fluxes, the results obtained with the Reynolds-Stress Model are used.

Smooth walls

The calculated flow field for the smooth wall channel is presented in Fig. 4 and Fig. 5 On the left hand side in Fig. 4 the lines of constant velocities at the entrance of different sections are shown (see also Fig. 2 for the definition of the sections). With the assumed uniform velocity boundary condition at the entry, the boundary layer develops along the first leg. At the end of the first leg the flow is still not fully developed (Fig. 4b), but the influence of the turn is already visible by a high velocity core that is slightly shifted towards the inner surface. Due to the strong curvature of the bend and the expanding area within section E, the flow is shifted towards the outer side. Therefore, the highest velocity in the cross section mid plane at 90° (Fig. 4c) can be found on the outer side wall. The highest velocity in the turn, caused by secondary flow effects and the pressure gradients in the turn can be observed on the side walls. At the end of the turn (Fig. 4d) the velocity at the side walls is decreased while the velocity at the outer wall is further increased. Within the second leg this high velocity core spreads out towards the center while the velocity in the core decreases. At the end of section I a almost normal duct flow has developed again. The high velocity core region is only slightly shifted against the outer wall.

On the right hand side in Fig. 4 the secondary flow vectors (projection of the velocity vectors) are shown in the same cross sections. Note that the scale of the vectors in Figs 4a and 4e is 10 times bigger than the scale in Figs. 4b to 4d. The developing boundary layer, mentioned above can be seen by a secondary flow, that is oriented from the walls towards the center of the channel. In section E the flow is accelerated (low pressure) at the inner side and decelerated (high pressure) at the outer side. This pressure gradient leads to a secondary flow in the side wall boundary layer from the outer side to the inner side (see also Fig 5). The secondary flow forms two counter rotating vortices in the turn (Fig. 4c). In the outer corner of section E the deceleration leads to a small region of reversed flow (Fig. 5). Note that the secondary flow rapidly decreases in the second leg.

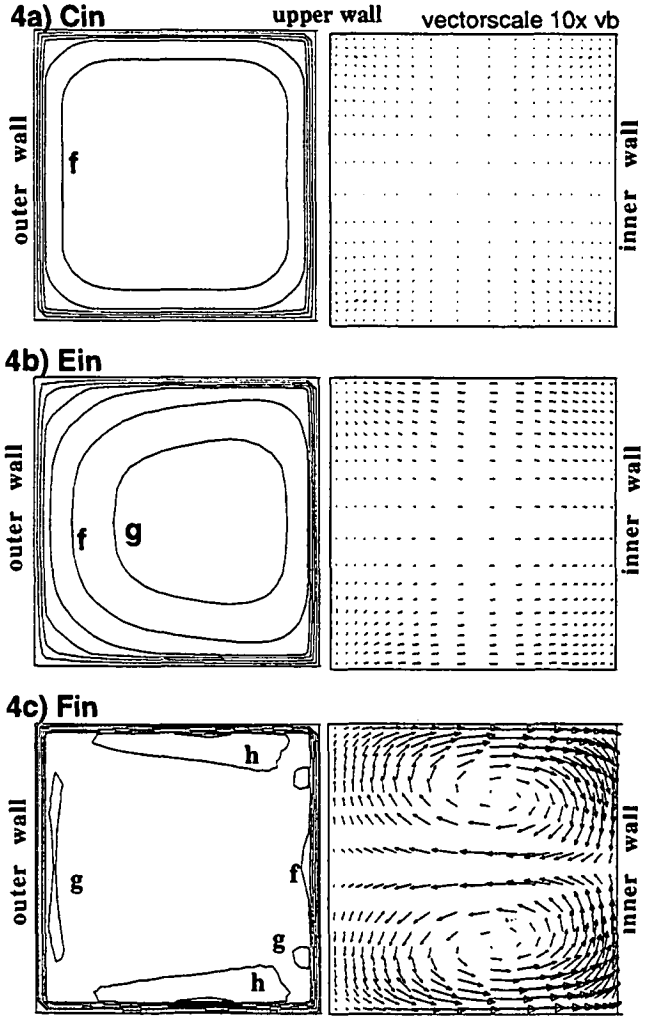

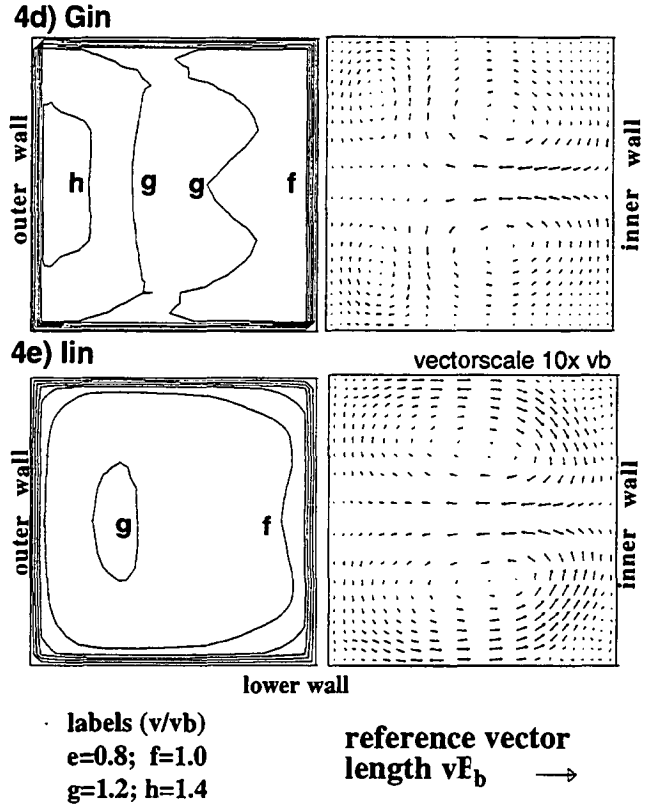

Fig. 4: Contours of constant velocities and secondary flow in cross sections

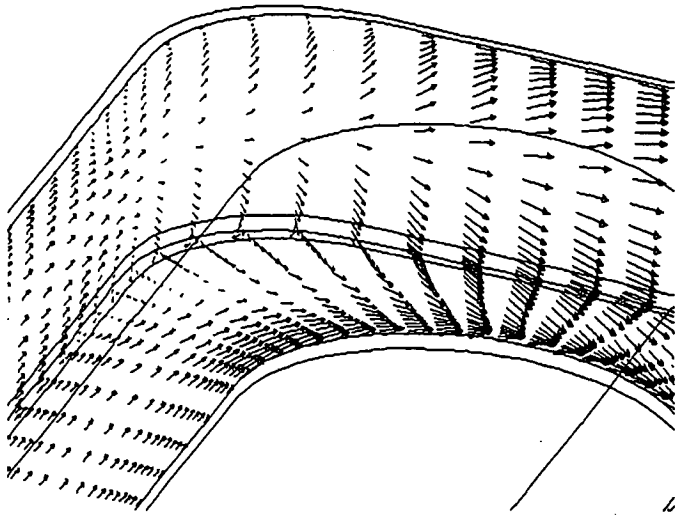

Fig. 5: Velocity vectors at planes 5 percent d_H from the wall

In Fig. 6, the calculated lines of constant heat flux are shown on the inner wall and in the turn. The highest heat flux arises at the beginning of section A (first heated section), where the greatest temperature difference occurs between isothermal wall and the fluid. With increased fluid temperatures, the heat flux decreases in stream wise direction. The heat flux has his lowest value in the turn at the first edge on the outer side due to the reversed flow. At about 90° in the turn, two regions with a high heat transfer rate are visible:

- on the side walls, caused by the high secondary flow
- on the outer wall, caused by the core flow that impinges against that wall.

In the second straight section, the heat flux is higher on the outer wall, due to the core flow being shifted towards the outer side.

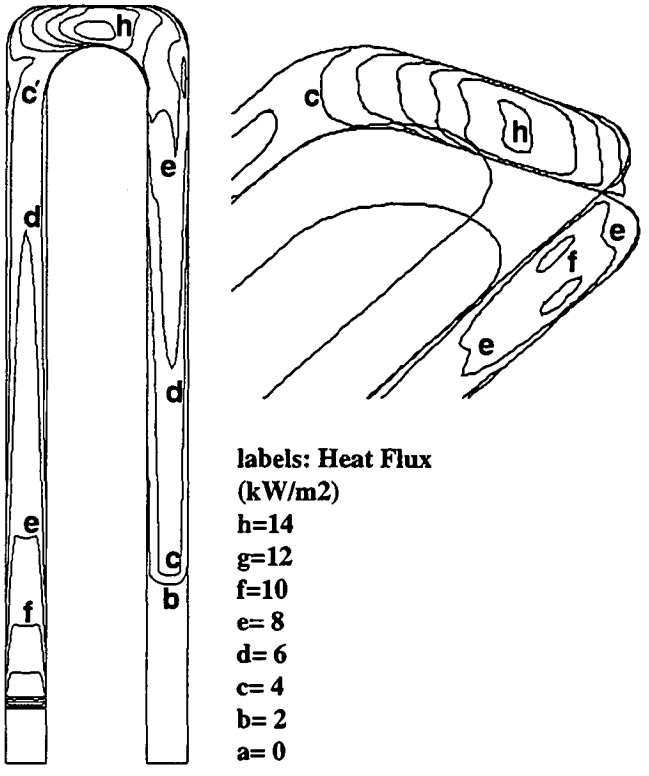

Fig. 6: Contours of constant heat flux at the walls

The segment - averaged Nusselt numbers on the inner, outer and one side wall are shown for all sections in Fig. 7. The segment-averaged Nusselt number was computed for all heat transfer section using the local mass averaged temperature T_b of each section. The transport properties were related to the average of the bulk and the wall temperature. The Nusselt numbers that were used for the comparison between measurements and calculations are the side-averaged Nusselt numbers devided by the Nusselt number for a fully developed flow in a square duct Nu_∞ with the same hydraulic diameter and the same Reynolds number at the inlet. This Nusselt number is obtained from the Kays and Perkins (1973) correlation, i. e., $Nu_\infty = 0.0176 \cdot Re^{0.8}$ with a Prandtl number equal 0.72.

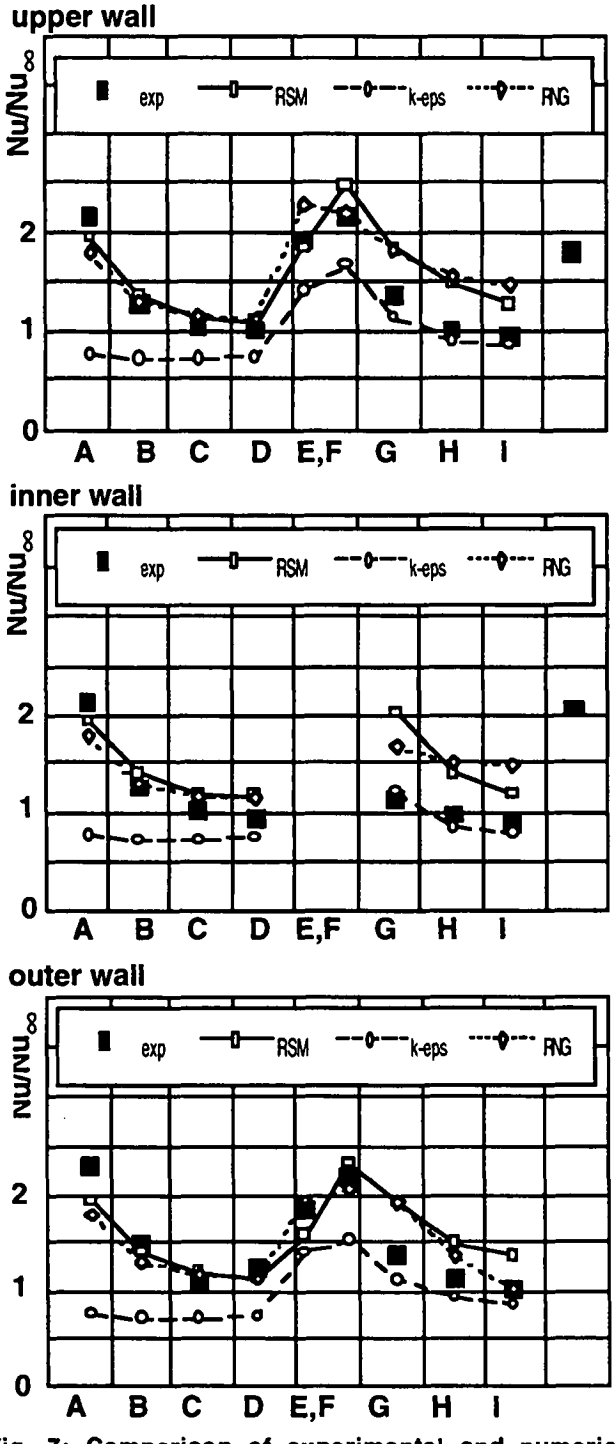

Fig. 7: Comparison of experimental and numerical segment-averaged Nusselt number distribution (smooth duct)

The experimental data and the numerical results for the three different turbulence models are plotted. The results are shown as heat transfer ratio, Nu/Nu_∞. The effects of location from the calculations that were discussed in Fig. 6 were also evident in the experimental results: Section A has the highest heat transfer, in sections B, C and D the heat transfer continuously decreases to a Nusselt number which is equal to Nu_∞ (equal to the Nusselt number in a fully developed duct flow). In the turn, the heat transfer increases to about $1.9*Nu_\infty$ in section E and to about $2.2*Nu_\infty$ in section F. Due to the fact that the experimental Nusselt numbers are averaged, the predicted local heat transfer variations are not visible. In the second leg, the Nusselt number decreases again down to about Nu_∞.

In the first passage, the Nusselt numbers predicted with both the RNG and RSM turbulence models agree with the experimental results. In the turn, the RNG model over predicts the average heat transfer in the first part (section E) but predicts the measured Nusselt number in the second half (section F). The RSM model prediction is in good agreement with the experiment in the first half of the turn but is higher than measured in the second half. The calculated heat transfer in the second passage is higher than the measured heat transfer for both turbulence models but has the measured characteristic of decreasing downstream of the turn. The k-ε model predicts a heat transfer in the first section which is much lower than that found in the experiments and the calculated Nusselt numbers are lower than measured in all sections and on all walls.

Fig. 8 presents the comparison of the measured and calculated pressure drop in all sections relative to the area-averaged dynamic head at the inlet. It is assumed that the effects of the different velocity inlet profiles between measurements and the calculations are diminished in section B. Therefore, the pressure in section B is used as reference pressure. The predicted pressure loss is within the uncertainty of the measurements for the calculations with k-ε and RSM, while the pressure drop with the RNG model in the turn is greater than measurement uncertainties.

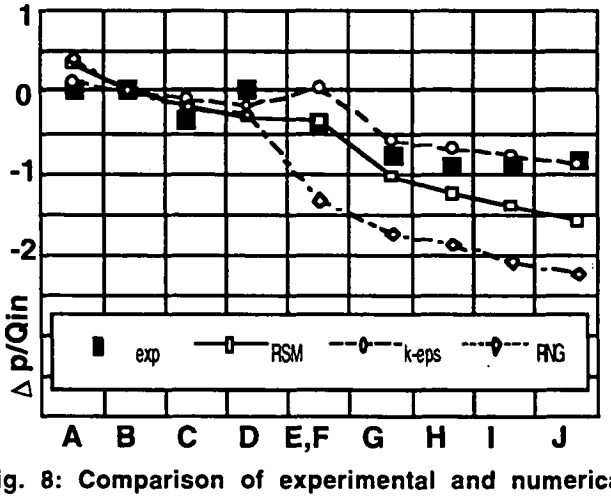

Fig. 8: Comparison of experimental and numerical static pressure distribution (smooth duct)

Walls with staggered, skewed ribs

The calculated flow field for the ribbed wall channel is presented in Figs. 9 and 10. After section B, the first ribbed section (Fig 9a), the flow is fully dominated by the influence of the ribs. Each rib acts like an obstacle that reduces the through flow area. Thus the velocity increases on top of the ribs and this leads

to a high velocity region behind the ribs. Due to the staggered positions of the ribs, these high velocity regions alternate between the upper and lower side walls. This effect is visible in both straight sections. In contrast to the smooth wall case, the velocity magnitude in the bend is almost uniform.

The secondary velocity vectors, plotted on the right hand side in Fig. 9, also clearly show the effects of the ribs. Due to the arrangement of the strips from the inner to the outer side in the first leg and from the outer to the inner side in the second leg, the flow is driven towards the outer side in the first straight section and towards the inner side in the second straight section, respectively. As a consequence two counter rotating vortices are formed.

The absolute velocity vectors in the vicinity of the walls between two ribs in the first leg are shown in Fig. 10b. Note that the magnitude of the secondary flow and the mean flow are of the same order. The flow characteristics in the turn are shown in Fig. 9c and Fig. 10a. The two counter rotating vortices due to the ribs in the first leg are entering the turn (Fig. 9b). The orientation of the vortices on the sidewalls are towards the outer side. The same effects, that were discussed for the smooth wall channel leads to the two additional vortices in the turn. The orientation of these vortices (towards the inner wall) is contrary to the incoming vortices. At the end of the turn, only the vortices that are induced by the curvature of the turn remain. As a result of these effects, two important differences between the ribbed and non ribbed case occur:

- due to the counteracting effects of the two pairs of vortices, the magnitude of the secondary flow in the turn is lower for the ribbed wall case.
- due to the transport of mass towards the outer side at the entrance of the turn, the reversed or separated flow in the first corner on the outer wall of the turn does not occur for the ribbed wall case (see Fig. 10a).

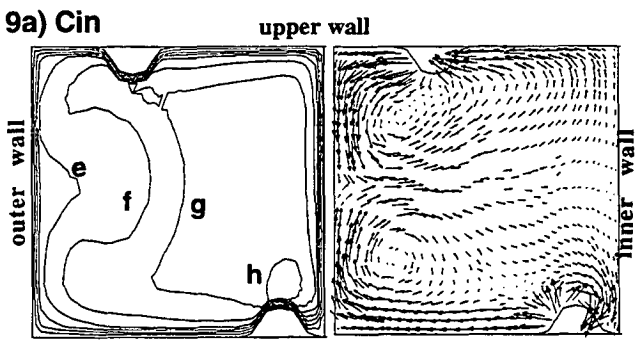

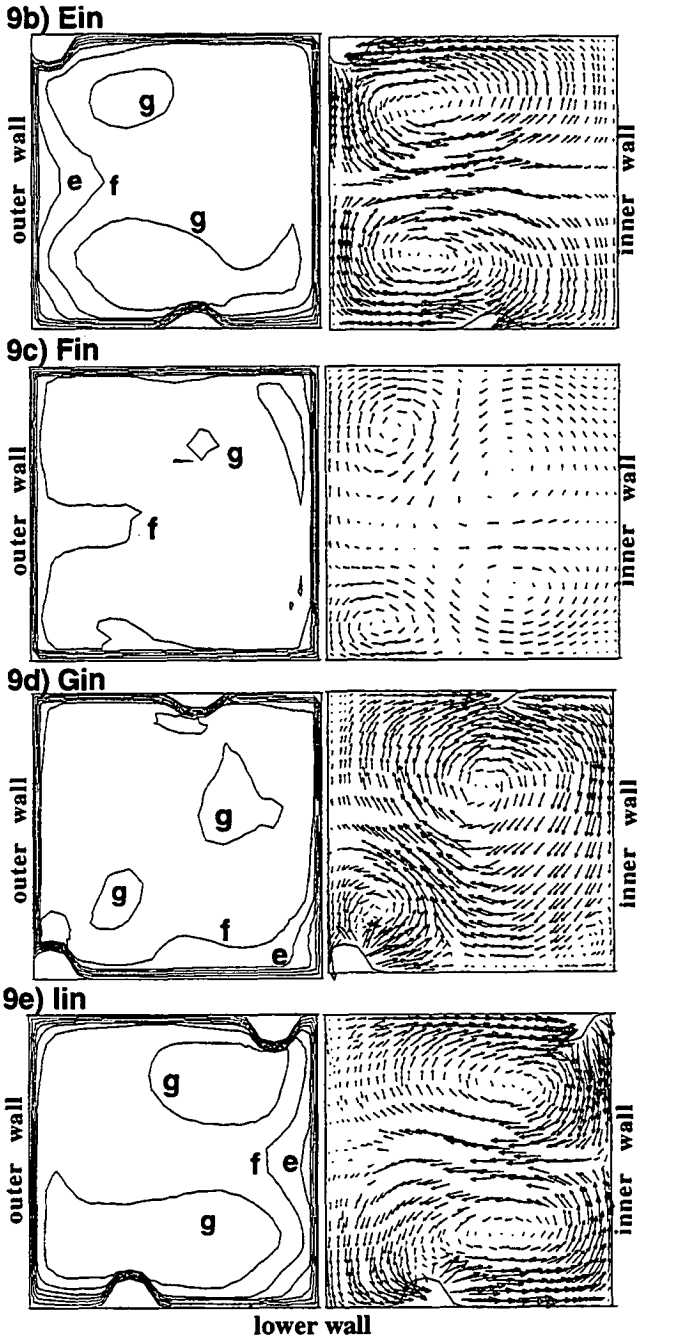

Fig. 9: Contours of constant velocities and secondary flow in cross sections of the ribbed duct

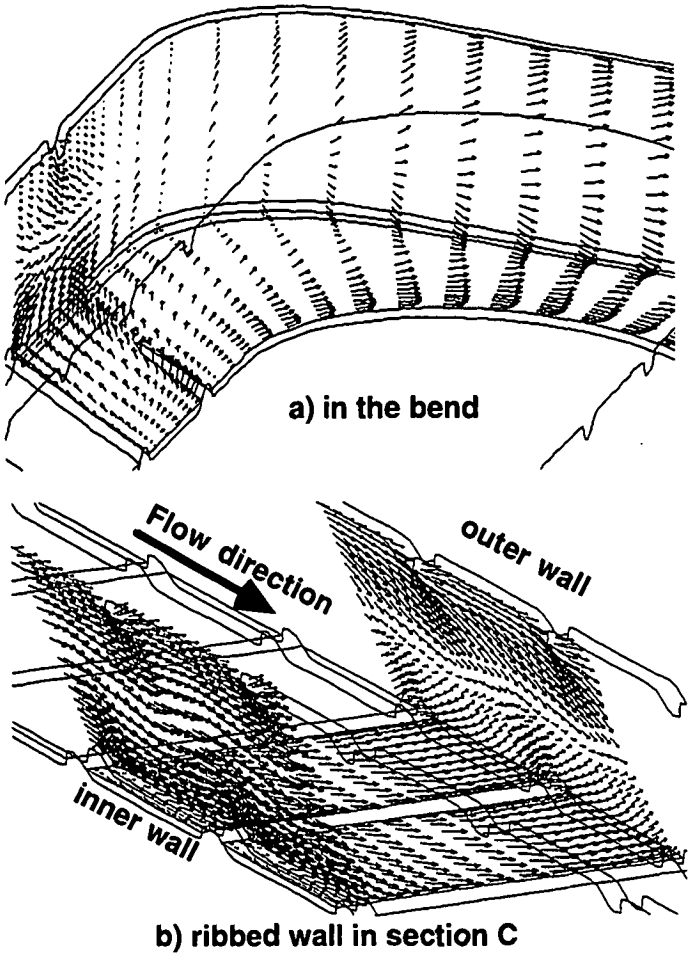

Fig. 10: Velocity vectors at planes 5 percent dH from the wall

The calculated lines of constant heat flux for the ribbed model are shown in Fig. 11. Although the structure of the isolines in both legs is somewhat irregular, the patterns are similar for all straight sections with ribs. In comparison to the smooth wall case, the levels of the heat flux on the inner and outer wall are about twice as high. A detailed pattern of the heat flux between two ribs on the lower side is shown in Fig. 11c. In between two ribs, a high heat transfer region is visible. This heat transfer peek is attributed to the location of the rib on the opposite (upper) side wall. The rib on the upper side wall apparently causes the flow to be driven towards lower side. This leads to a higher velocity and therefore to the increased local heat transfer. Due to the increased velocity, the heat flux increases on the top of each rib and is predicted to be 25 to 30 percent higher than the peak heat transfer between the ribs. In the turn region the differences in the flow field between the ribbed and the smooth wall case, described above, are believed to cause the following differences in the heat transfer:

- the heat transfer in the middle of the turn is lower due to the lower secondary flow.
- the heat transfer in the first corner on the outer wall is higher due to the absence of the reversed flow.

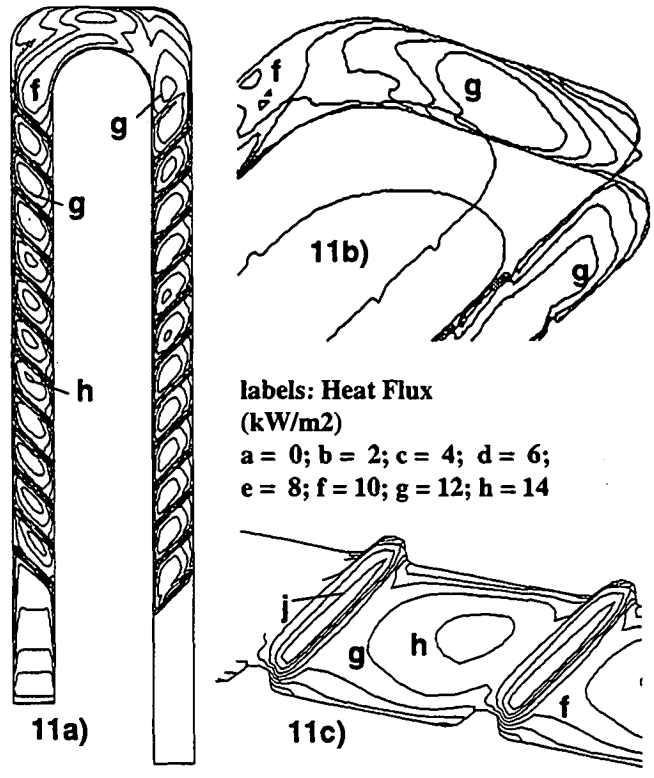

Fig. 11: Contours of constant heat flux at the walls

The comparison between the measured and the calculated wall section averaged Nusselt numbers for all sections at the different walls are shown in Fig. 12. In comparison to results for the duct with smooth side walls (also plotted as a reference with light gray symbols), the predicted heat transfer character is changed significantly. For the smooth walls, the Nusselt number decreases continuously on all walls in the first leg down to approximately $Nu/Nu_\infty = 1$.

For the ribbed walls, the Nusselt numbers increases downstream of the inlet on all sides. On the ribbed walls, the Nusselt numbers rapidly increases to about $3^* Nu_\infty$. On the inner and outer walls, a more moderate increase of the Nusselt numbers occurred. The effects of the flow that are responsible for the different heat transfer results in the turn , i.e., low Nusselt numbers in the first turn section and high Nusselt numbers in the second turn section for the case with smooth walls and the reverse situation for the case with ribbed walls, were discussed previously for the numerical results in Fig. 11.

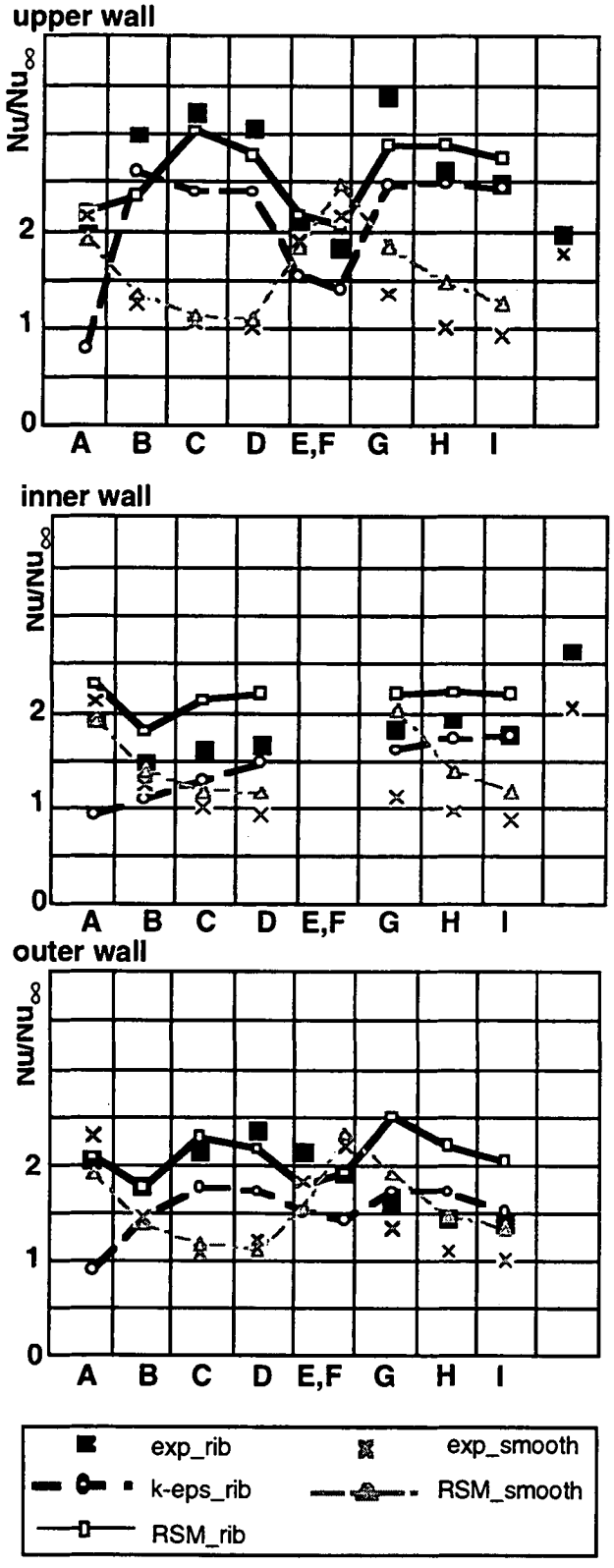

Fig. 12: Comparison of experimental an numerical segment-averaged nusselt Number distribution (ribbed duct)

In the second leg, the Nusselt numbers increases only on the inner side caused by the orientation of the ribs and the related flow effects. On all other walls in the second leg, the Nusselt numbers decreases downstream of the turn for both the smooth and ribbed wall models.

The predicted Nusselt numbers using RSM clearly shows all differences in the heat transfer characteristic between the smooth wall and the ribbed wall case. In the first leg the agreement between the calculations and the measurements is good on the upper wall and the outer and the inner wall. However, the RSM has problems in predicting the heat transfer level downstream of the bend, especially along the outer wall. In the upstream sections, the RSM over-predicts the heat transfer level along the inner wall. The predictions using the k-ε model for the ribbed wall model are too low in general as were the results for the case with smooth walls.

The calculated pressure distribution along the ribbed duct are compared to the measured pressure distribution in Fig. 13. The predicted pressure losses are approximately the same for both the RSM and the k-ε turbulence models. The agreement with the measurements is very good.

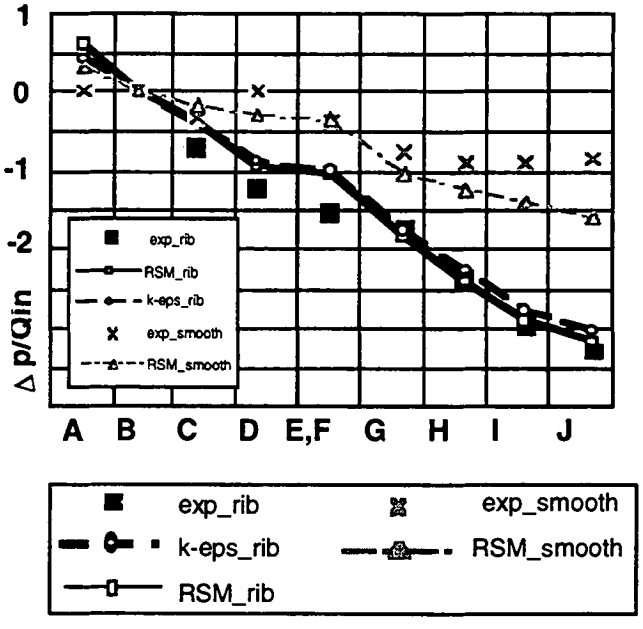

Fig. 13: Comparison of experimental and numerical static pressure distribution (ribbed duct)

SUMMARY OF RESULTS

A numerical study of the flow and heat transfer in stationary U-shaped cooling channels with smooth wall and with skewed ribs was performed using the FLUENT code. Three different turbulence models were used. The comparison between previous

measurements and the numerical results were used to judge the ability of numerical predictions for heat transfer calculations.

The main findings of the study may be summarized as follows.

a) The major flow effects are captured correctly with all turbulence models
   - in the turn, two counter rotating vortices are formed, induced by the pressure gradient between the inner and outer surface. The orientation of the vortices on the sidewalls are towards the inner wall.
   - in the ribbed sections, two vortices are generated. With the given orientation of the ribs, the flow is driven towards the outer side in the first leg and towards the inner side in the second leg, respectively.

b) The pressure drop in the straight sections and in the turn are well predicted with k-e and the Reynolds-stress- model for both the smooth and the ribbed coolant channel, while the predicted pressure drop in the turn is too high with the RNG model.

c) The agreement of the heat transfer predictions with the experimental results depends strongly on the turbulence model used.
   - the heat transfer predicted with the standard k-ε model is lower in general on all surfaces than the experimental results for both wall configurations.
   - with smooth walls, the agreement between the predicted heat transfer and the measurements is good for the RSM and low-Re-RNG models. However, the predicted heat transfer coefficients in the second leg are greater than those measured.
   - with the ribbed side walls, the predicted heat transfer using RSM is in good agreement with the measurements and all major variations in the heat transfer distribution were predicted correctly. The level of the predicted Nusselt numbers are too high in the second leg.

The results of the present study show that accurate heat transfer predictions can be achieved with modern turbulence models. The numerical predictions from a detailed analysis of the flow field leads to a better understanding of the physics and turbulent transport mechanisms in the cooling channels of turbine blades. When equally satisfactorily agreement with rotating heat transfer experiments can be obtained with numerical predictions for similar flow conditions and geometries, the gas turbine designer will have a useful and, probably, a very cost effective design verification tool.

ACKNOWLEDGMENTS

This study was supported by ABB as part of a Corporate Research project and as a Diploma thesis for Uwe Tomm, RWTH Aachen.

REFERENCES

Abuaf, N and Kercher, D. M., 1994, "Heat Transfer and Turbulence in a Turbulated Blade Cooling Circuit", ASME Journal of Turbomachinery, Vol. 116, pp. 169-177.

Bo, T., Iacovides, H., and Launder, B. E., 1995, "Convective Discretization Schemes for the Turbulence Transport Equations in Flow Predictions Through Sharp ,U-Bends", 1995, Int. J. of Num. Methods. for Heat & Fluid Flow, Vol. 5, pp. 33-48.

FLUENT User's Guide, 1995, Version 4.3, Vol. I-IV, Fluent Deutschland GmbH.

Hajek, T. J. Wagner, J. H., Johnson, B. V., Higgens, A. W., and Stueber, G. D.,1991, "Effects of Rotation on Coolant Passage Heat Transfer: Volume I-Coolant Passages with Smooth Walls", NASA Contractors Report 4396, Vol. I.

Iacovadies, H. and Launder, B. E., 1995, "Computational Fluid Dynamics Applied to Internal Gas-Turbine Cooling: A Review", Inter. J. Heat and Fluid Flow, Vol.. 16, pp. 454-470.

Johnson, B. V., Wagner, J. H., and Stueber, G. D., 1993, "Effects of Rotation on Coolant Passage Heat Transfer: Volume II-Coolant Passages with Trips Normal and Skew to the Flow", NASA Contractors Report 4396, Vol. II.

Johnson, B. V., Wagner, J. H., Steuber, G. D., and Yeh, F. C., 1994, "Heat Transfer in Rotating Serpentine Passages with Trips Skewed to the Flow", ASME Journal of Turbomachinery, Vol. 116, pp. 113-123.

Kays, W. M., Perkins, H. C., 1973, "Forced Convection, Internal Flow in Ducts", from Handbook of Heat Transferred Rohsenow, W. M. and Hartnett, J. P., McGraw Hill, pp. 7-28 and 7-33.

Launder, B. E., 1989, "Second-Moment Closure: Present ... and Future?", Inter. J. Heat Fluid Flow, Vol. 10, No. 4, pp. 282-300.

Launder, B. E., Reece, G. J., and Rodi, W., 1975, "Progress in the Development of a Reynolds Stress Turbulence Closure", J. Fluid Mech., Vol. 68(part 3), pp. 537-566.

Launder, B. E. and Spalding, D. R., 1972, "Lectures in Mathematical Models of Turbulence", 1972, Academic Press, London, England.

Launder, B. E. and Spalding, D. R., 1973, "The Numerical Computation of Turbulent Flows", Imperial College of Science and Technology, London, England.

Prakash, C., and Zerkle, R.,1992, "Prediction of Turbulent Flow and Heat Transfer in a Radial Rotating Square Duct", ASME Journal of Turbomachinery, Vol. 114, pp. 835-846.

Prakash, C., and Zerkle, R.,1993, "Prediction of Turbulent Flow and Heat Transfer in a Ribbed Rectangular Duct with and without Rotation", ASME preprint 93-GT-206.

Rodi, W., 1984, "Turbulence Models and their Application in Hydraulics", Delft, The Netherlands, IAHR.

Taylor, C., Xia, J. Y., Medwell, J. O., and Morris, W. D., 1991, "Numerical Simulation of Three Dimensional Turbulent Flow and Heat Transfer within a Multi-Ribbed Cylindrical Duct", ASME Preprint 91-GT-8.

Wagner, J. H., Johnson, B. V., and F. C. Kopper, 1991, "Heat Transfer in Rotating Serpentine Passages With Smooth Walls", ASME Journal of Turbomachinery, Vol. 113, pp. 321-330.

Yakhot, V., Orszag, S. A., 1986, "Renormalisation Group Analysis of Turbulence", I. Basic Theory, J. of Sci. Comput., Vol. 1, No. 1, pp. 1-51.